JOURNAL OF SOLID STATE CHEMISTRY 116, 256–264 (1995)

Structural Models for Cobalt–Tin Oxide Thin Films

L. E. Depero,[1] P. Levrangi, and G. Sberveglieri

Dipartimento di Chimica e Fisica per i Materiali, Università di Brescia, Via Branze 38, 25123 Brescia, Italy

Received November 29, 1993; in revised form October 12, 1994; accepted October 17, 1994

Thin films of ternary compounds with formula $Sn_{1-x}Co_xO_y$ ($0 < x \leq 0.15$) were studied by X-ray diffraction. The diffraction patterns from the new compounds with $x < 0.20$ are similar to those obtained from pure SnO_2 thin films. The relationships between rutile (SnO_2) and the spinel structure of Co_2SnO_4 are discussed by describing them in similar unit cells, as obtained by the transformations

$$\begin{pmatrix} 0 & -1 & 0 \\ 0 & 1 & 1 \\ -1 & 0 & 0 \end{pmatrix} \text{ and } \begin{pmatrix} 1 & 0 & -1 \\ 0 & -1 & 1 \\ -1 & -1 & -1 \end{pmatrix},$$

respectively. For $x = 0.20$, a new phase appears, closely related to SnO_2. For this new phase all the reflections in the corresponding powder pattern can be indexed with an orthorhombic unit cell, in which the parameters ($a = 9.400$ Å, $b = 9.557$ Å, and $c = 6.33$ Å) are about twice those of SnO_2. Different models for this new phase are derived and calculated diffraction patterns are compared with those observed. © 1995 Academic Press, Inc.

1. INTRODUCTION

The most common technologies for preparing solid-state gas sensors are based on thick film and thin-film techniques (1, 2). Codeposition studies of various metals and SnO_2 have recently been reported (3–5). In particular, a new method for thin-film gas sensors was recently developed (6, 7). This process, called rheotaxial growth and thermal oxidation (RGTO), is based on the sputtering of metal thin films on a substrate, maintained at a temperature higher than the metal melting point, followed by annealing in oxygen performed for obtaining the metal oxide.

In a previous work, the structure of ternary compounds $Sn_xFe_yO_z$, obtained by the RGTO technique, was studied (8). Even for high Fe contents, the only phase that could be detected in the X-ray diffraction pattern was that of SnO_2. In view of the similarity of the ionic radii of Sn^{4+} (0.71 Å) and Fe^{3+} (0.64 Å) and of the Pauling electronegativities ($Fe^{3+} = 1.8$, $Sn^{4+} = 1.8$), an explanation for this fact was proposed, based on the substitution of Fe for Sn in the rutile-type structure of SnO_2. Moreover, Fe^{3+} in its oxides prefers the octahedral coordination, like that of the rutile-type structure (9), and, in the only known structure of Fe and Sn mixed oxides ($Fe_{3-x}Sn_xO_4$), Sn substitutes for Fe in the octahedral sites of a spinel-like structure (10).

In general, derivation and refinement of structural models for these materials are difficult, due to the simultaneous presence of two or more phases (that of the support materials and those constituting the thin film) and to preferred orientation effects. However, the relevance of this modeling to the understanding of conduction and growth mechanisms in these materials is so great that it should be tried even if only qualitative results can be expected, in view of the above-mentioned difficulties.

The aim of this work is to propose structural models for new ternary compounds $Sn_xCo_{1-x}O_y$ prepared by the RGTO technique. In this case, a diffraction pattern different from that of pure SnO_2 was obtained only for the sample with highest Co content (20 at.%). In the derivation of these models, it is basic to detect common elements belonging to all possibly related structures. For this reason, in what follows, we will transform the conventional rutile and spinel unit cells into a couple of similar cells, in which the relationships between the two structures can be more clearly recognized. The proposed models are strictly related to these structures.

2. EXPERIMENTAL

Al_2O_3 supports were used to deposit the metal thin films. During the thermal evaporation the pressure in the deposition chamber was maintained at about 7.5×10^{-7} Torr, by means of a cryogenic pump. Sn was first deposited with a deposition rate of 6–7 Å/sec. During the deposition the substrate temperature, controlled by a thermocouple, was kept at $T = 533$–543 K, i.e., at a temperature higher than the Sn melting point ($T = 505$ K). Co was deposited without breaking the vacuum with a deposition rate of 1.5 Å/sec. During this second deposition, the sub-

[1] To whom correspondence should be addressed.

0022-4596/95 $6.00

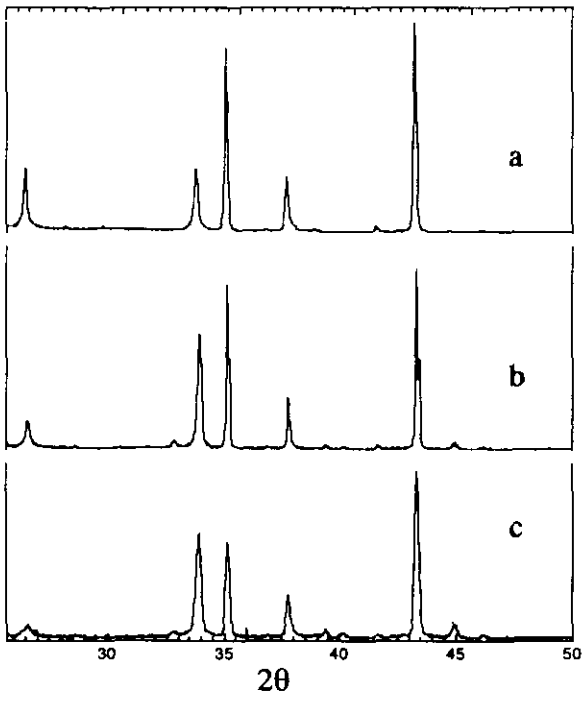

FIG. 1. X-ray diffraction patterns of (a) SnO_2 reference thin film sample on Al_2O_3; (b) ω–2θ scan of a thin film sample with a 20% Co atomic content; (c) same as in (b) with an offset ω-angle of 12.5°.

TABLE 1
Cell Parameters and Volumes for the Considered Phases and the Refined Model

	a (Å)	b (Å)	c (Å)	V (Å^3)
Co_3O_4	8.083	8.083	8.083	528
Co_2SnO_4	8.646	8.646	8.646	646
SnO_2	4.747	4.747	3.185	72
Model	9.400	9.557	6.334	569

TABLE 2
Parameters and Volumes of the Cells Transformed According to Matrices [1] and [2]

	a (Å)	b (Å)	c (Å)	α	β	γ	V (Å^3)	Me–Me
Co_3O_4	11.43	11.43	14.00	90°	90°	120°	1584	2.858
Co_2SnO_4	12.23	12.23	14.98	90°	90°	120°	1939	3.057
SnO_2	5.17	5.71	4.74	90°	90°	112°	143	3.185
	(× 2)	(× 2)	(× 3)	90°	90°	112°	1716	
	11.42	11.42	14.21					
	(× 2)	(× 2)	(× 2)	90°	90°	112°	1144	
	11.42	11.42	9.48					
$Sn_xCo_yO_z$	11.46	11.46	9.40	90°	90°	113°	1138	3.167

Note. Me–Me along the octahedral chains are reported in column 8.

TABLE 3
Indices, 2θ Positions, and Relative Intensities Calculated for Al_2O_3, SnO_2, and Model I

Al_2O_3			SnO_2			Model I		
h k l	2θ	I (%)	h k l	2θ	I (%)	I (%)	$2\theta_{obs}$[a]	I_{obs} (%)
							19.40	2
1 0 2	25.6	60					25.58	30
			1 1 0	26.6	100	22	26.60	27
							28.62	1
							32.87	7
			1 0 1	33.9	80	100	33.92	100
1 0 4	35.2	93					35.16	82
							36.88	1
1 1 0	37.8	43	2 0 0	38.0	23	59	37.79	28
			1 1 1	39.0	5	4	38.99	1
							39.41	2
							40.16	1
							41.69	2
1 1 3	43.4	98	2 1 0	42.7	2	1	43.37	95
							44.96	5
2 0 2	46.2	1					46.19	1
			2 1 1	51.8	82	76	51.79	16
2 0 4	52.6	49					52.56	46
			2 2 0	54.8	20	31	54.79	3
1 1 6	57.5	100	0 0 2	57.9	10	15	57.51	112

[a] The integrated intensities are calculated by using APD software (Philips).

TABLE 4
Crystal Data and Atomic Positions x, y, z for the Considered Models

a = 9.557 Å
b = 9.400 Å
c = 6.334 Å
Space group = $Fdd2$

For all models:				
Sn	0	0	0	
Sn	0	0	0.5	
O	0.1535	0.1535	0	
O	0.1535	0.1535	0.5	
Model II				
Co	0.25	0	0	
Model III				
Co	0	0.25	0.25	
Co	0.25	0.25	0	
Model IV				
Co	0.2	0	0	
Model V				Occupancy
Co	0.2	0	0.25	0.5
Co	0	0.2	0.25	0.5

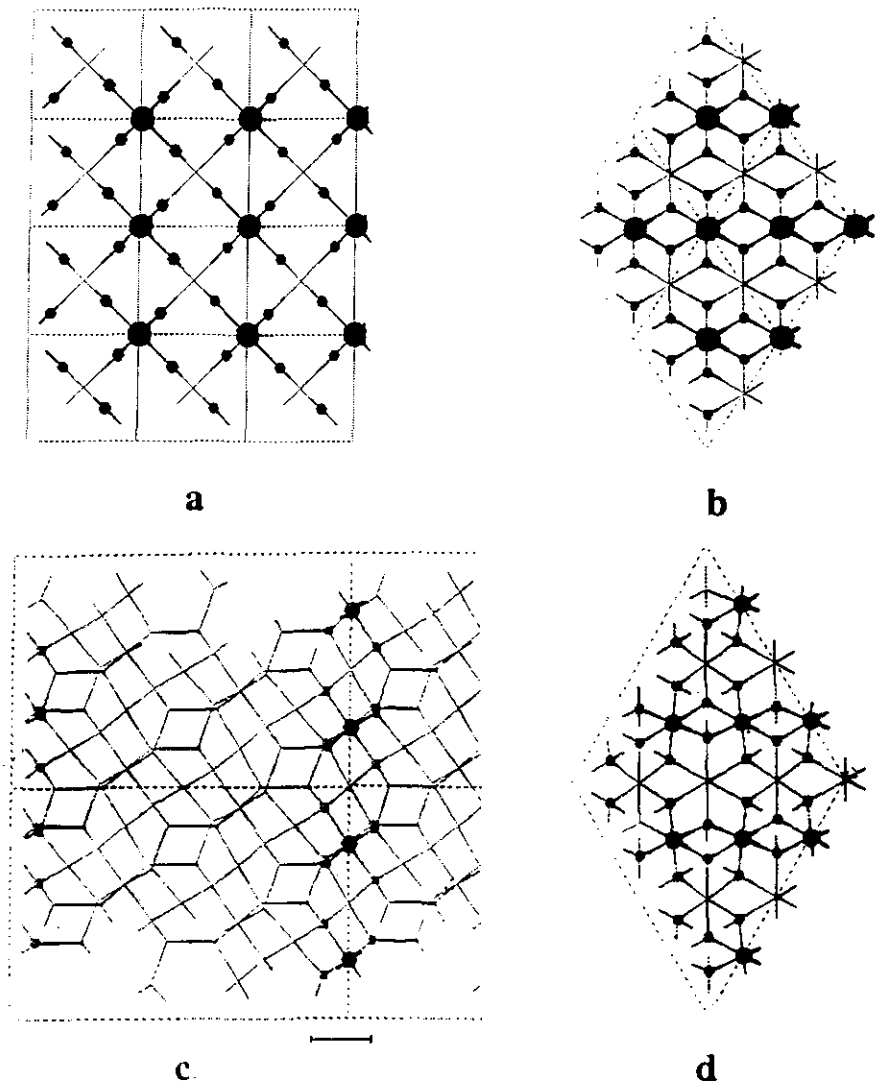

FIG. 2. Projections of the rutile and spinel structures; the large and small circles represent metal and oxygen atoms respectively. (a) Rutile structure projected along the [110] direction of the cell transformed by matrix 1; (b) rutile structure projected along the c-axis of the cell transformed as in (a); (c) spinel structure projected along the [110] direction of the cell transformed by matrix [2]; (d) projection along the c-axis of the slab indicated in (c).

strate temperature was kept at 463 K. The Sn layer was about 3600 Å thick, while the Co thicknesses were chosen to obtain a Co atomic content between 0.01 and 0.20. The evaporation rate of the thin films as well as their masses was monitored by a calibrated quartz microbalance placed nearby the Al_2O_3 supports.

A Pt meander sputtered on the back side of the Al_2O_3 substrate was used either as a heater or as a temperature sensor. The total power needed to heat the whole system at 673 K was about 0.93 W. The thermal oxidation of both the Sn and Co layers was achieved by annealing in an oxygen flow.

The X-ray diffraction measurements were performed on a Philips MPD 1880 automated powder diffractometer with graphite-monochromated Cu$K\alpha$ radiation in the Bragg–Brentano parafocusing geometry. While we checked for preferred orientation, the ω- and 2θ-axes were rotated independently, thus allowing for an "offset" angle.

Modeling and simulations were performed using the CERIUS program on an IBM RISK 6000 work station (11).

3. RESULTS AND DISCUSSION

A reference thin-film sample, with Sn deposited on an alumina substrate, was studied by X-ray diffraction after annealing in air. A relatively well crystallized SnO_2 phase was identified (Fig. 1a, Table 1, and Table 3) (12).

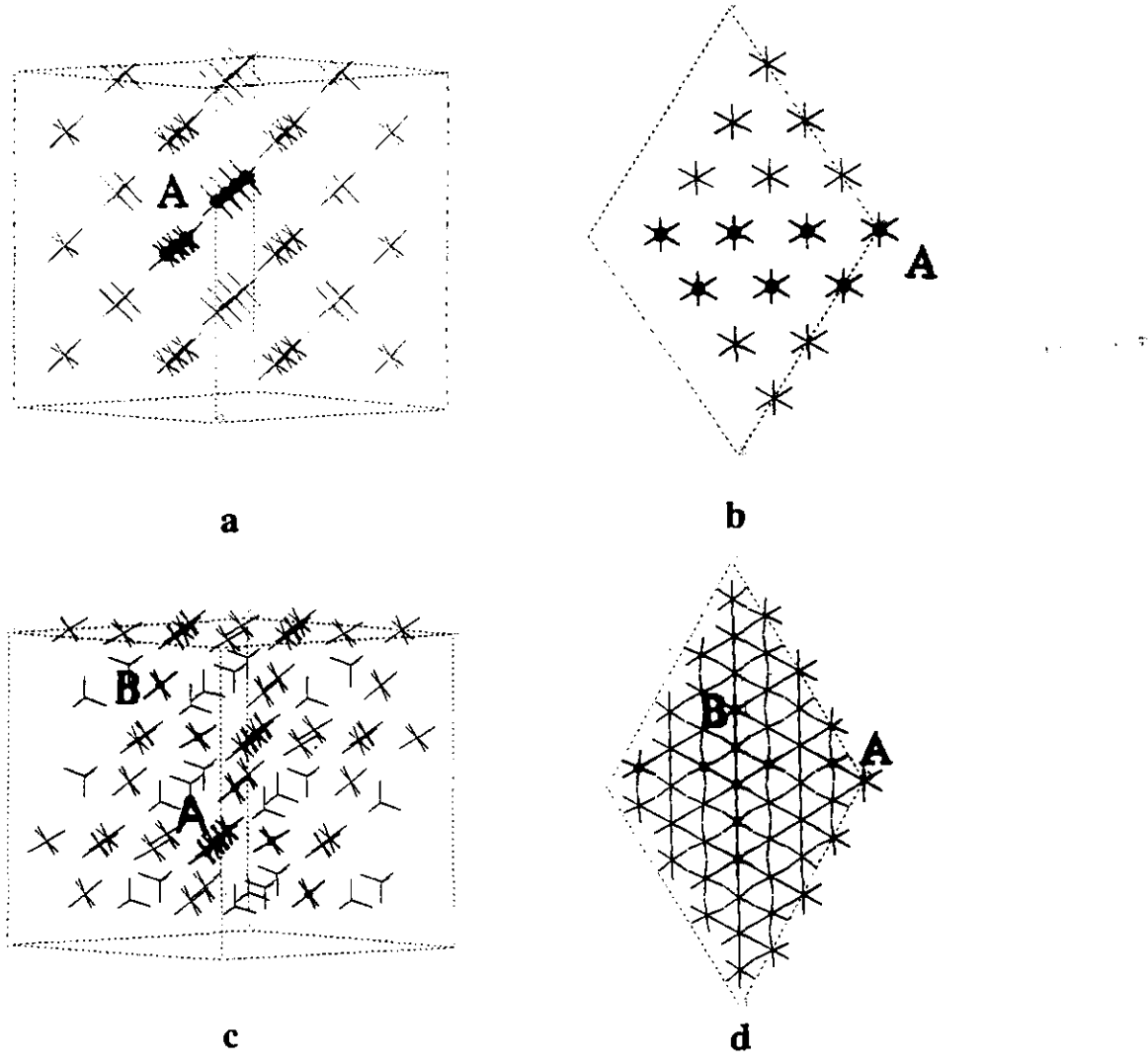

FIG. 3. Prospective and projection views of rutile (a and b) and spinel (c and d) structures, where only the metal positions and the spikes indicating the coordination directions are drawn. In (a) and (c), the threefold symmetry axes of all the coordination polyhedra are clearly parallel to the c-axes of the transformed cells. Octahedral chains of both A and B types (see text) are indicated in bold.

The samples with a 0.5, 1, 10, 15 at.%. Co content show X-ray diffraction patterns identical to that of pure SnO_2. As in the case of $Sn_xFe_yO_z$ thin films studied previously (8), here substitution of Co for Sn in the rutile structure of SnO_2 also is possible and can justify the similarity of the observed patterns. On the contrary, the diffraction pattern of the sample with a 20 at.% Co content shows interesting differences (Fig. 1b), the most important one being the inversion of the intensity ratio between the reflection at a 2θ value of about 26.6° and that at 33.8°, corresponding to the 1 1 0 and 1 0 1 reflections in the SnO_2 phase, respectively. A possible explanation for this inversion could be found in the preferred orientation effects of the thin film. This possibility was checked by remeasuring the diffraction pattern with a ω-offset of 12.5° (Fig. 1c). In the Al_2O_3 phase, preferred orientation is clearly shown by the important variation of the intensity ratio of the 1 0 4 and 1 1 3 reflections at 2θ values of 35.2° and 43.4°, respectively. Therefore, the fact that the intensity ratio of the 1 0 1 and 1 1 0 reflections of the SnO_2 phase remains approximately constant strongly indicates the absence of preferred orientation effects in this case. Thus any variation observed in the pattern of the sample with a content of 20 at.% Co with respect to the reference SnO_2 film can be attributed to structural changes undergone by this material.

In the Inorganic Crystal Structure Database (12), only one structure of Sn–Co mixed oxides is reported, i.e., that with the formula Co_2SnO_4. In this spinel-like structure, the octahedral sites are randomly occupied by both

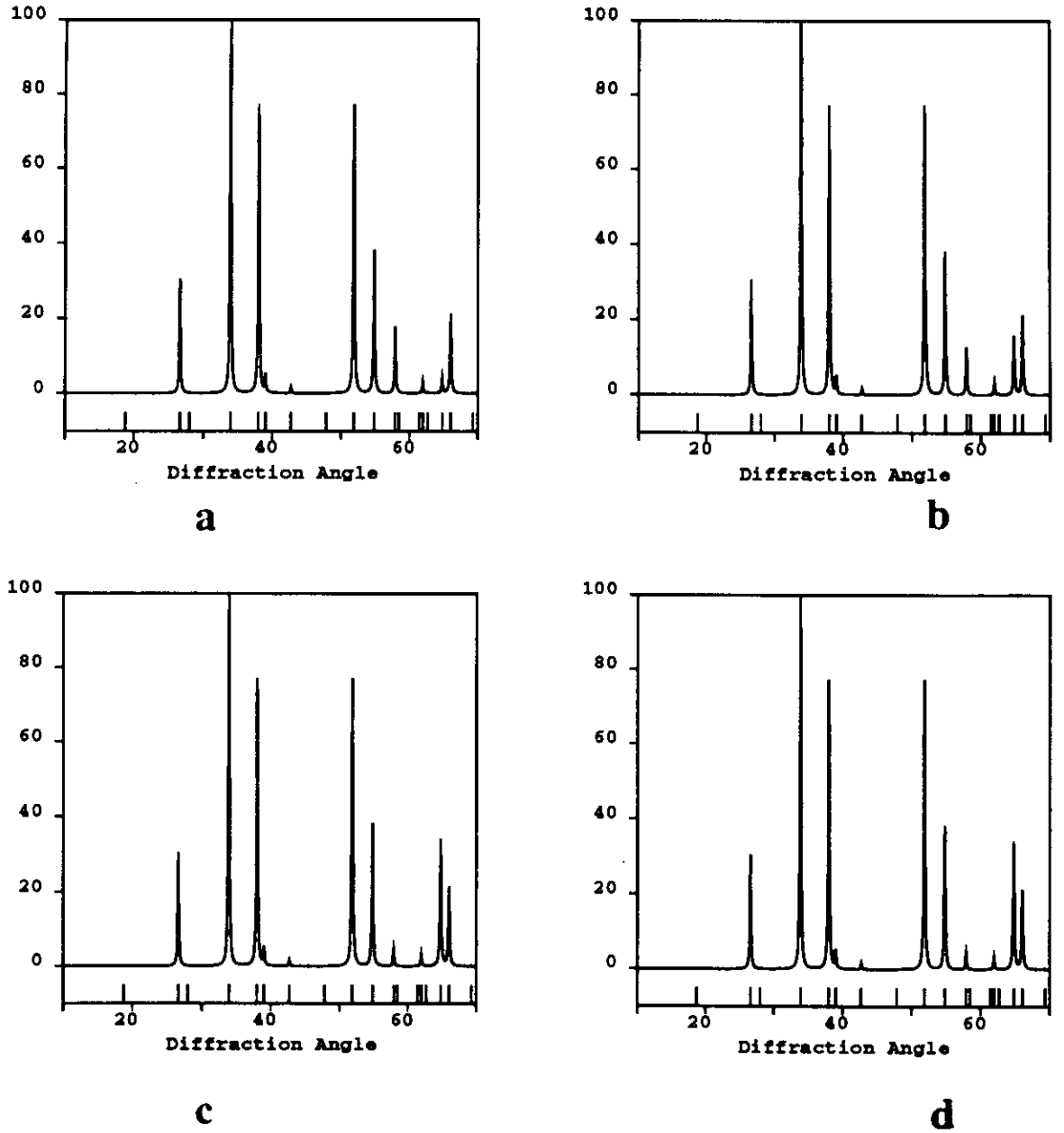

FIG. 4. Simulated patterns taking into account the cooperative shifts of all the Co atoms (see text), corresponding to (a) $z = 0.0$, (b) $z = 0.1$, (c) $z = 0.2$, and (d) $z = 0.3$.

the Sn and Co cations, while only Co ions occupy the tetrahedral sites. The spinel-like structure is typical of many other mixed oxides such as $Fe_{2.5}Sn_{0.5}O_4$, $Co_{0.90}Mn_{0.10}O_4$, and Co_3O_4, where both octahedral and tetrahedral coordinations are used by the cations, while the oxygen atoms have tetrahedral coordination. Also the rutile-like structures are common in transition metal oxides, where cations occupy only octahedral sites and the oxygen atoms have threefold coordination. In fact, these two structures are more strictly related to each other than it is commonly believed, and this is better realized if one describes them in similar cells by performing the axis transformations

$$\begin{pmatrix} 0 & -1 & 1 \\ 0 & 1 & 1 \\ -1 & 0 & 0 \end{pmatrix} \qquad [1]$$

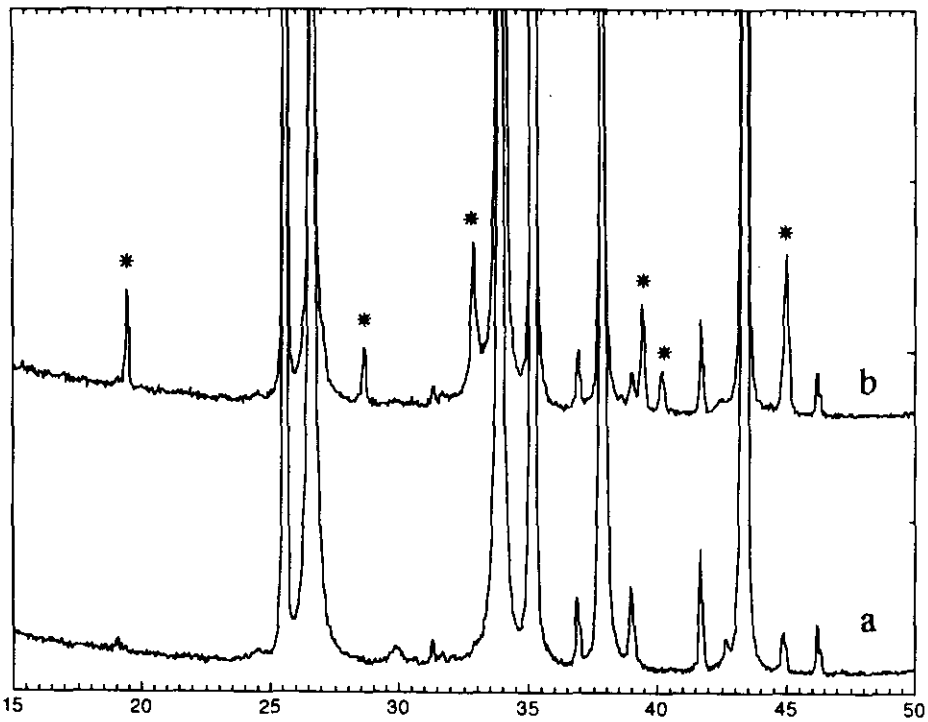

FIG. 5. Enlarged (a) and (b) patterns from Fig. 1. The small peaks of the new phase are indicated by asterisks.

and

$$\begin{pmatrix} 1 & 0 & -1 \\ 0 & -1 & 1 \\ -1 & -1 & -1 \end{pmatrix} \quad [2]$$

for the rutile and the spinel-like structures, respectively. In Table 1, the conventional cell parameters of the studied materials, as given in the literature (12), are reported, while the cell parameters as determined by applying these axis transformations are given in Table 2. The volumes of the transformed cells of Co_3O_4 and Co_2SnO_4 are three times those of the conventional unit cells, while the transformed cell volume of SnO_2 is two times that reported in the literature. It is interesting to note that, as indicated in Table 2, axis lengths of the new Co_3O_4 cell can be obtained from those of the SnO_2 cell by multiplying a and b by 2 and c by 3. In fact the main difference between the latter two cells is the g angle which decreases from 120° in Co_3O_4 to 112° in SnO_2. These geometrical features correlate with important structural similarities, as indicated by the fact that, since, in both structures, chains of octahedra run along lines parallel to the [110] direction, the *Me–Me* distances decrease with increasing Co content and can be easily calculated from the geometry of the transformed cells (Table 2).

The two different structures appear to be uncorrelated in the [110] projections shown in Figs. 2a and 2c, but if only the slab indicated in Fig. 2c is projected along the c-axis the similarities between the two structures can be better appreciated (Figs. 2b and 2d). This similarity is based on the fact that in both structures one of the three-fold symmetry axes of all the coordination polyhedra (both octahedra and tetrahedra) is parallel to the c-axis of the transformed cells, as shown in Fig. 3, where only the metal positions and the spikes indicating the coordination directions are drawn. Moreover, while in both structures one can identify chains of octahedra running parallel to the [110] direction (Set A of Fig. 3), in the case of the spinel structure another set of chains (Set B, Figs. 3c and 3d) runs along the [−112] direction and, therefore, in the projection along the c-axis, is perpendicular to the chains of set A.

From the structural relationships found for these compounds and from the fact that the stronger reflections in the pattern of $Sn_xCo_yO_z$, with higher Co contents, have the same $2q$ positions as those of pure SnO_2, we started our model derivation with the assumption that this new phase is strictly related to that of SnO_2.

In the first structural model (Model I), Co atoms are inserted into the voids of the rutile structure at (0.5, 0, 0) with an occupancy of 0.5. The simulated pattern of Fig. 4a is obtained and the calculated intensities are reported in Table 3. The main feature observed in the pattern of

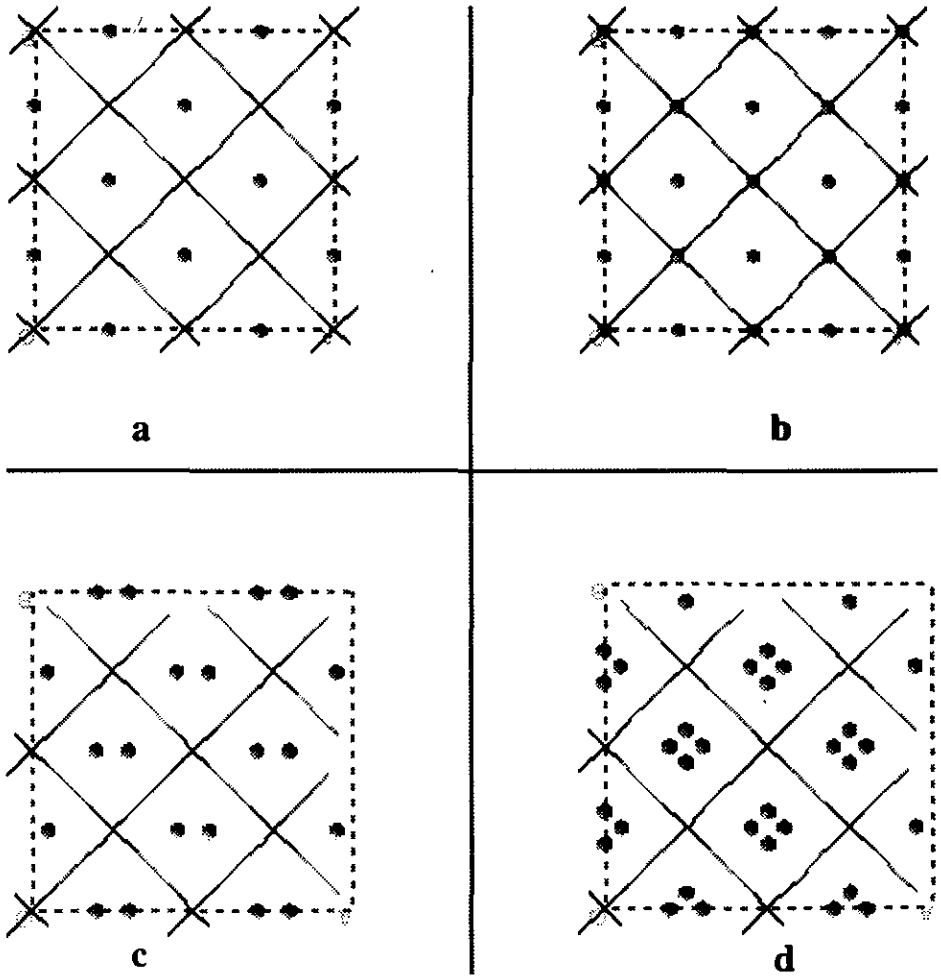

FIG. 6. Projections along the c-axis of (a) Model II, (b) Model III, (c) Model IV, and (d) Model V. In the frame of the rutile structure, the inserted Co atoms are shown.

the $Sn_xCo_yO_z$ phase, i.e., the inverted ratio of the reflections at 26.6° and at 33.8°, is justified by this simple model. Another significant difference between the calculated SnO_2 pattern and the simulated pattern of Model I is given by the intensity of the 200 reflection which is coincident with the 110 reflection of the Al_2O_3 support. Since, as mentioned above, the support pattern is strongly affected by preferred orientation, one cannot use this information in modeling. It is interesting to note that, after removing all the symmetry constraints by changing the space group $P4_2/mnm$ (No. 136) to $P1$, any possible cooperative shift of all the Co atoms along the c-axis implies no significant change in the simulated pattern up to the 2θ position of the 002 reflection, as shown in Fig. 4. This constitutes further evidence of the difficulties encountered in model refinements of these materials. Moreover, the same argument can be used as strong evidence for the occupation of interstitial sites by Co in the rutile structure. Thus, of course, the 2θ range should be as large as possible, but, unfortunately, any possible use of the thin-film higher-angle reflections is impossible due to their broadening. A reasonable explanation to this broadening is offered by a disordered distribution of Co atoms, as can be deduced by the above considerations.

However, the presence of several small peaks in the pattern in Fig. 5b allows one to try some tentative modelling. Indeed, the indexing of all these small peaks is possible by doubling all the cell parameters. The observed 2θ positions and those calculated on the basis of the refined unit cell are reported in Table 5 below. Orthorhombic refinement of the unit cell parameters (Table 1) leads to a small difference between a and b. Further evidence for an orthorhombic cell is given by the fact that the 202 reflection cannot be fitted by a single pseudo-Voigt func-

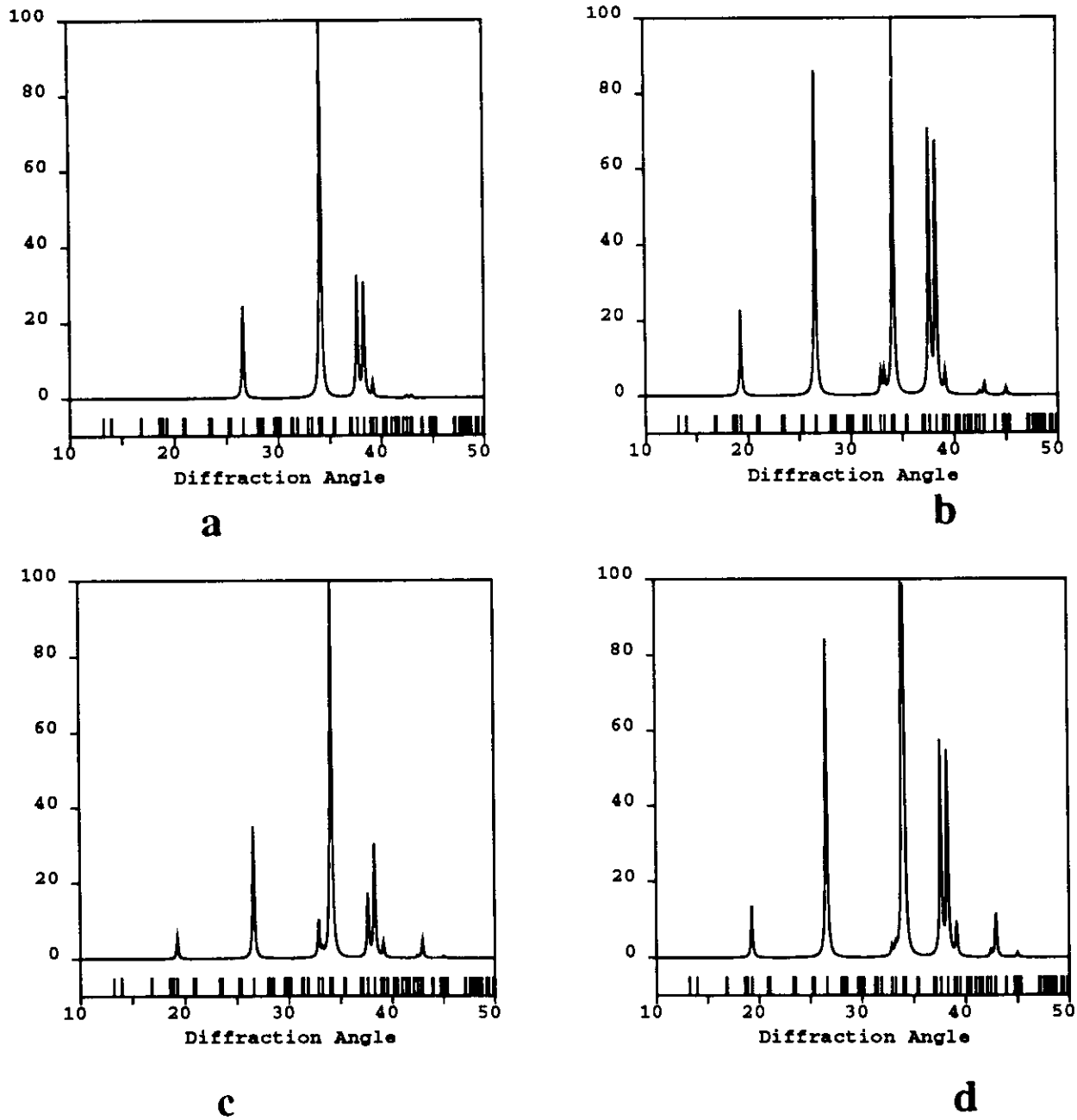

FIG. 7. Simulated patterns corresponding to the models shown in Fig. 6.

tion and that a quite good fitting was obtained with two functions, which can be attributed to the 202 and 022 reflections. In Table 2, the values obtained by transforming the refined cell by matrix [1] are reported. The *a* and *b* parameters of this new cell (11.46 Å) are slightly larger than twice that of SnO_2 (11.42 Å) and smaller than that calculated for the spinel structure of Co_2SnO_4 (12.23 Å). The γ angle (113°) is very close to that of SnO_2 (112°). If one supposes that, also in the new phase, octahedral chains run along the [110] direction of the transformed cell (type A, Fig. 3) as in the rutile and spinel structures, the *Me–Me* calculated distance is 3.167 Å (Table 2), an intermediate value between those of Co_2SnO_4 and SnO_2.

The structure of the new phase in its orthorhombic cell (Table 1) can be described in the *Fdd*2 space group with the atomic coordinates reported in Table 4. Four models were tested in the same space group. The atomic coordinates for these models are reported in Table 4, and the corresponding calculated intensities are given in Table 5. In Figs. 6 and 7, the related projections of these models

TABLE 5

Indeces, 2θ Positions, and Relative Intensities Calculated for the Considered Models Compared with Corresponding Observed Values

			Model					
			II	III	IV	V		
h	k	l	2θ	I (%)	I (%)	I (%)	I (%)	$2\theta_{obs}$	I_{obs} (%)
1	1	1	19.28		22	6	16	19.40	2
2	2	0	26.60	24	85	35	97	26.60	27
0	3	0	28.46					28.62	1
3	1	1	32.88		6	10	3	32.87	7
1	3	1	33.25		5	1	3		
2	0	2	33.96	7	1	11	100	33.92	100
0	2	0	34.14	100	100	100	99		
3	2	1	36.88					36.88	1
4	0	0	37.65	33	70	17	67	37.79*	28
0	4	0	38.30	31		31	64		
2	2	2	39.14	4	67	4	11	38.99	1
1	4	0	39.45					39.41	2
3	0	2	40.13					40.16	1
1	3	2	41.62					41.69	2
4	2	0	42.44	1	1	1	2		
2	4	0	42.88	1	1	1	2	43.37*	95
3	3	1	42.93		3	5	13		
1	1	3	45.02		2	1	2	44.96	5

Note. * indicates superposition with Al_2O_3 peaks.

along the c-axis and the diffraction simulations are shown. Model IV better justifies the observed pattern.

Since for the smaller Co contents the diffraction patterns are very similar to that of pure SnO_2 and since in the Co_2SnO_4 structure the Co atoms occupy both octahedral and tetrahedral sites, it is very likely that in the new phase Co and Sn are actually mixed in the cation sites.

Rietveld refinements of these models were attempted, but we did not have any significant improvement in the R-factor, since alumina is always present with some preferred orientation and too many correlated parameters need to be refined.

ACKNOWLEDGMENT

One of us (L.E.D.) is grateful to Marcello Zocchi for help in revising the paper.

REFERENCES

1. V. Lantto and P. Romppainen, *Surf. Sci.* **192,** 243 (1987).
2. G. Sberveglieri, G. Faglia, S. Groppelli, and P. Nelli, *Sensors Actuators B* **8,** 179 (1992).
3. M. Flueli, R. Spycher, P. Stadelmann, P. Buffat, and J. P. Borel, *J. Microsc. Spectrosc. Electron.* **14,** 351 (1989).
4. P. J. Hewitt, D. A. Jefferson, G. R. Millward, and K. Tsuno, *JEOL News* **27E(I),** 2 (1989).
5. M. Labeau, B. Gautheron, F. Cellier, M. Vallet-Regi, E. Garcia, and J. M. Gonzalez Calbet, *J. Solid State Chem.* **102,** 434 (1993).
6. G. Sberveglieri, G. Faglia, S. Groppelli, P. Nelli, and A. Camanzi, *Semicond. Sci. Technol.* **5,** 1231 (1990).
7. G. Sberveglieri, G. Faglia, S. Groppelli, and P. Nelli, *IEEE Digest Tech. Pap. (91CH2817)* **5,** 165 (1991).
8. P. Bonzi, L. E. Depero, F. Parmigiani, C. Perego, G. Sberveglieri, and G. Quattroni, *J. Mater. Res.* **9,** 1250 (1994).
9. A. F. Wells, "Structural Inorganic Chemistry." Oxford Univ. Press, Oxford, 1984.
10. C. D. Jega-Mariadassau, F. Basile, P. Poix, and A. Michel, *Ann. Chem. (Paris)* **73,** 15 (1973).
11. CERIUS Version 3.2 User Manual: Molecular Simulations. Cambridge, 1993.
12. Inorganic Crystal Structure Database (ICSD). Gmelin-Institut für Anorganische Chemie and Fachinformationszentrum (FIZ) Karlsruhe, 1993.